PWM Converter Integrating Switched Capacitor Converter and Series-Resonant Voltage Multiplier as Equalizers for Photovoltaic Modules and Series-Connected Energy Storage Cells for Exploration Rovers

Masatoshi Uno, *Member, IEEE*, and Akio Kukita

***Abstract*— Power systems for exploration rovers tend to be complex as three separate converters are necessary; in addition to a main dc-dc converter and cell equalizer for rechargeable energy storage cells, an equalizer for photovoltaic (PV) modules is desirably equipped in order to preclude negative impacts of partial shading. This paper proposes the PWM converter integrating voltage equalizers for PV modules and energy storage cells. The proposed integrated converter comprises a switched capacitor converter (SCC), PWM buck converter, and series-resonant voltage multiplier (SRVM) that perform PV equalization, power conversion from the PV modules to the load, and cell equalization, respectively. Three converters can be integrated into a single unit with reducing the total switch count, achieving not only system-level but also circuit-level simplifications. The derivation procedure of the integrated converter is explained, followed by the operation analysis. Experimental tests were performed using series-connected supercapacitor (SC) modules and solar array simulators to emulate a partial shading condition. With the integrated converter, the extractable maximum power from the PV modules significantly increased while voltage imbalance of SC modules was adequately eliminated, demonstrating the integrated performance of the proposed converter.**

***Index Terms*—Equalization, integrated converter, series-resonant voltage multiplier (SRVM), switched capacitor converter (SCC).**

I. Introduction

Since the space shuttle, the most popular manned space vehicle, retired in 2011, various nations have launched unmanned space programs for deep space and planetary exploration using planetary probes and exploration rovers. Especially for exploration rovers, active research and development efforts aiming for the moon and Mars exploration are underway. The development of rovers faces new challenges, such as 1) significantly reduced power generation of photovoltaic (PV) strings due to partial shading generated by a pan camera, and 2) the requirement of further downsizing and lightening.

The photo of the moon exploration rover under development in Japan is shown in Fig. 1 as an example. The pan camera, an indispensable component for planetary surface exploration, is usually equipped on the top of the rover's body and nearly always casts a shadow over the solar panels, generating so-called 'partial shading.' Partial shading on a PV string comprising multiple PV modules/substrings (hereafter simply call modules) connected in series is a major stumbling block to the improved energy utilization. In a partially-shaded PV string, shaded modules are less capable of producing current, and hence, individual module characteristics are significantly mismatched depending on the degree of shading. The mismatch in PV module characteristics is known to create multiple maximum power points (MPPs), including one global and multiple local MPPs, in the string's P–V characteristic that trigger significant reduction in power generation and hinder ordinary MPP tracking (MPPT) algorithms.

To cope with the partial shading issues, distributed MPPT systems shown in Fig. 2(a), in which modules are individually controlled by module integrated converters (MICs), have been employed [1], [2]. Nowadays, differential power processing (DPP) converters and voltage equalizers that provide power transfer paths between adjacent modules [3]–[13] or between a string and shaded modules [14]–[17], as shown in Figs. 2(b) and (c), are vigorously studied and developed as a powerful alternative solution. With these converters, a fraction of generated power of unshaded modules is transferred to shaded ones so that all modules operate at the same voltage or even at each MPP, virtually unifying all module characteristics even

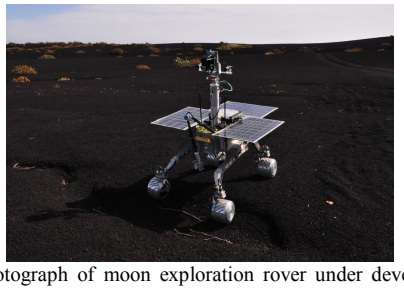

Fig. 1. Photograph of moon exploration rover under development in Japan.

Manuscript received August 7, 2016, revised November 1, 2016; accepted December 21, 2016. This work was supported partly by the Ministry of Education, Culture, Sports, Science, and Technology through Grant-in-Aid for Young Scientists (B) 25820118.

M. Uno is with the Faculty of Engineering, Ibaraki University, Hitachi 316-8511, Japan (e-mail: masatoshi.uno.ee@vc.ibaraki.ac.jp).

Akio Kukita is with the Institute of Space and Astronautical Science, Japan Aerospace Exploration Agency, Sagamihara 252-5210, Japan (email:kukita.akio@jaxa.jp).

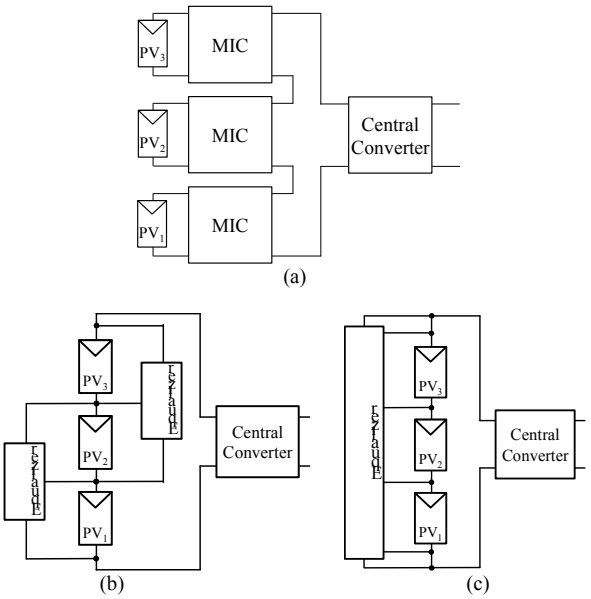

Fig. 2. PV system architectures: (a) Distributed MPPT, (b) adjacent module-to-module equalization, (c) string-to-module equalization.

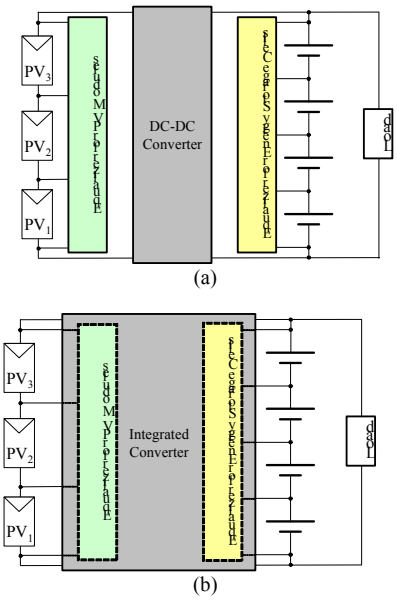

Fig. 3. Architectures of sun-regulated spacecraft power systems: (a) Conventional system using separate converters, (b) proposed integrated converter system.

under partial shading conditions. Although partial shading issues can be precluded with distributed MPPT systems, DPP converters, or voltage equalizers, PV systems tend to be complex as numerous converters are necessary in addition to the central converter, as can be seen in Fig. 2. This tendency is undesirable for exploration rovers because the increased number of converters naturally increase the system complexity and mass of the power system.

In the meantime, an energy storage source using rechargeable batteries or supercapacitors (SCs) is also indispensable for rovers to operate at night or under a shadow of rocks, craters, etc. on the moon and Mars surface. In general, energy storage sources, such as lithium-ion batteries (LIBs) and SCs, consisting of series-connected cells/modules (hereafter simply call cells unless otherwise noted) have issues of cell voltage imbalance. Voltages of series-connected cells are gradually imbalanced due to non-uniformity among individual cell characteristics in terms of capacity/capacitance, self-discharge rate, internal impedance, and environmental temperature. Mismatch in capacity/capacitance originating from manufacturing tolerance, for example, is generally around a few percent. Mismatch in self-discharge rate is dependent on temperature distribution in a system because self-discharge is accelerated at high temperatures. In a voltage-imbalanced energy storage source, cells deteriorate at different rate — the higher the voltage, the faster the cell ages —, resulting in accelerated aging as a whole system. A degradation rate of supercapacitors, for example, is not only dependent on temperature [18], [19] but also reportedly doubled for every 100 mV increase [20]. In addition, as cells are cycled in series, some cells having the highest and lowest voltages might be over-charged and -discharged, respectively, posing serious concerns about safety because operation beyond the safety boundary specified by manufacturers may cause hazardous consequences.

Cell voltage equalizers are widely used to prevent the voltage imbalance issues and to ensure years of safe operation. Various kinds of cell equalizers have been proposed and developed [21]–[36], and their topologies and operation principles are very similar to those of DPP converters and voltage equalizers for series-connected PV modules — most voltage equalization techniques were originally developed and used for battery equalization. This fact implies that cell voltage equalizers for energy storage cells pose the same issues as the DPP converters and voltage equalizers for PV systems; numerous voltage equalizers are necessary, increasing the system complexity.

Fig. 3(a) illustrates a typical spacecraft power system architecture based on so-called ‘sun-regulated bus system’ where an energy storage source is directly connected to a load. The main dc-dc converter is active only when PV modules can supply power, while the energy storage source directly discharges to the load at night or eclipse periods. This example architecture consists of three PV modules, four energy storage cells, and string-to-module equalizers for both PV modules and energy storage cells. The separate equalizers for PV modules and energy storage cells are necessary in addition to the main dc-dc converter, suggesting there is still room for improvement from the perspective of system-level simplification. In other words, if these three converters were partly or completely unified, the system would be significantly simplified and lightened by reducing the component count.

In our prior work, we have focused on a system-level simplification technique by integrating multiple converters into a single unit and have proposed a PWM converter integrating voltage equalizers for energy storage cells and PV modules [37]. The notional system architecture using the proposed integrated converter is illustrated in Fig. 3(b); functional parts of

equalizers for PV modules and energy storage cells are contained in the integrated converter. Three separate converters can be integrated into a single unit without introducing complex control technique, hence easily achieving system-level simplification.

This paper presents the extended and fully-developed work about the integrated converter proposed in the previous work [37]; more detailed analyses, derivation of a dc equivalent circuit, and detailed experimental and simulation results will be presented. The derivation procedure of the proposed integrated converter is explained in Section II, followed by the operation analysis and derivation of a dc equivalent circuit in Section III. Sections IV and V present experimental and simulation results, respectively.

II. Integrated Converter

A. Key Elements for Proposed Integrated Converter

The proposed integrated converter can be derived from the combination of a PWM buck converter, switched capacitor converter (SCC), and series-resonant voltage multiplier (SRVM), as shown in Fig. 4. The SCC and SRVM have been proposed and developed as a voltage equalizer for series-connected PV modules and energy storage cells, and their individual operations have been thoroughly analyzed in the literature. The SCC transfers power between adjacent two modules/cells so that module voltages are unified [12], [13]. The SRVM redistributes the input power to a module/cell having the lowest voltage in a string [38]. In the proposed integrated converter, the SCC and SRVM perform voltage equalization for PV modules and energy storage cells, respectively, while the buck converter plays a role of output voltage regulation.

The key elements shown in Fig. 4 produce or are driven by square wave voltages depicted in insets. Square wave voltages are generated at switching nodes in the PWM buck converter and SCC (nodes X–Z). In the PWM buck converter, a voltage across the inductor L is also a square wave voltage. Meanwhile, in conventional voltage equalizers using an SRVM, a square wave voltage is produced by a half-bridge inverter to drive the resonant tank in the SRVM [39]. These three elements can be integrated into a single unit if these square wave voltages are shared among them, as detailed in the next subsection.

B. Derivation of the Proposed Integrated Converter

In the PWM buck converter shown in Fig. 4(a), the operation can be regarded that the filter inductor L is driven by a square wave voltage produced by the switch Q and diode D_O. Meanwhile, the SCC also produces square wave voltage at its switching nodes X–Z. Hence, instead of using Q and D_O, the square wave voltage generated in the SCC can be utilized to drive the inductor L in the PWM buck converter, realizing the integration of the SCC and buck converter.

Similarly, the square wave voltage produced across L can also be utilized to drive the SRVM. Simply connecting the input of the SRVM to L of the buck converter can realize the integration of the PWM buck converter and SRVM, as reported in the previous study [38]. However, two separate magnetic components (i.e., L and transformer for the PWM buck converter and SRVM, respectively) are necessary, increasing the converter volume, mass, and cost. In the proposed integrated converter, on the other hand, L and transformer can also be integrated by utilizing the transformer's magnetizing inductance L_{mg} as a filter inductor for the PWM buck converter.

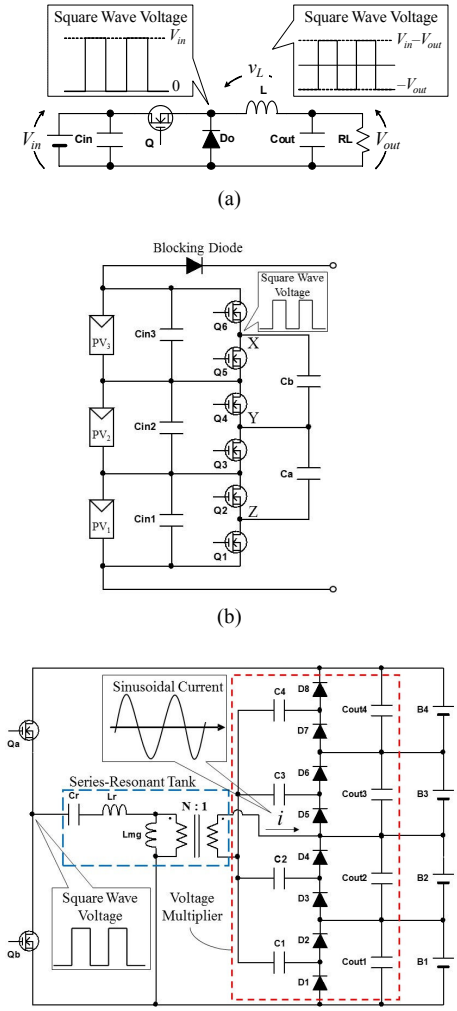

Fig. 4. Key elements for the proposed integrated converter: (a) PWM buck converter, (b) PV modules with switched capacitor converter (SCC) and blocking diode, (c) series-resonant voltage multiplier (SRVM).

On the basis of the aforementioned derivation procedure, the proposed integrated converter for three PV modules PV_1–PV_3 and four energy storage cells B_1–B_4 can be yielded as shown in Fig. 5. The SCC and PWM buck converter are integrated by sharing switches Q_5 and Q_6. In other words, the square wave voltage at the node X is utilized. Meanwhile, the PWM buck converter and SRVM share the primary winding of the transformer — the filter inductor L of the buck converter is replaced with L_{mg} of the transformer. A blocking diode is placed in series with the transformer primary winding in order to prevent reverse power flow into PV modules.

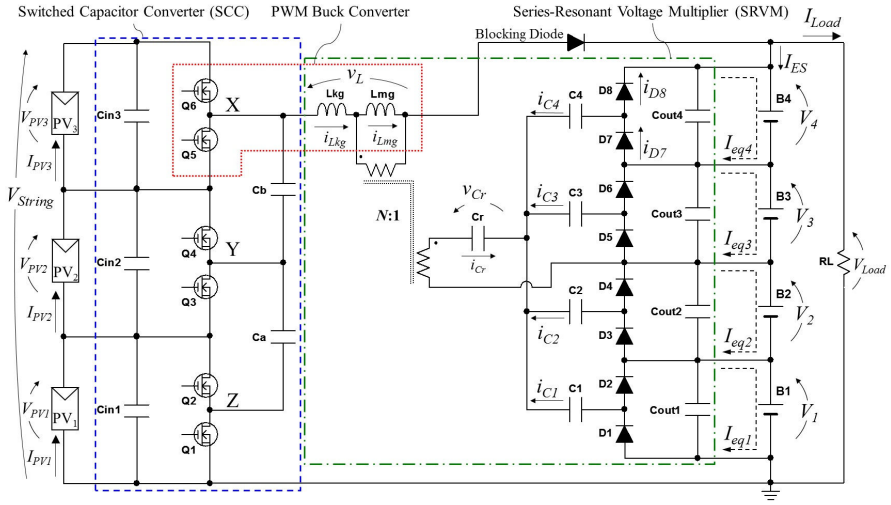

Fig. 5. Proposed integrated converter for three PV modules and four energy storage cells connected in series.

L_{mg} functions as a filter inductor for the PWM buck converter, while the leakage inductor L_{kg} resonates with the resonant capacitor C_r placed on the transformer secondary side. In order to obtain desirable inductances for L_{mg} and L_{kg}, a loosely-coupled transformer that is conventionally used for LLC resonant converters [40] would be best suitable. A resonant frequency f_r, an important parameter dictating a duty cycle variation range and cell voltage equalization performance, as will be discussed with (1) and (7), respectively, is dependent on L_{kg}. If L_{kg} cannot be precisely designed even with such transformers, f_r can be a desirable value by properly determining a value of the resonant capacitor C_r [see (2)].

In the integrated converter shown in Fig. 5, the square wave voltage generated at the switching node X is utilized to drive the primary winding of the transformer. Other switching nodes Y and Z can also be used although voltage step-down ratio differs, as will be discussed in Section III-B.

C. Major Features

The proposed integrated converter offers some major benefits. Three components (the PWM buck converter and equalizers for PV modules and energy storage cells) can be integrated into a single unit, achieving system-level simplification by reducing the component count. No additional feedback control loop is necessary for equalizers for PV modules and energy storage cells in the integrated converter system, thanks to the automatic equalization mechanisms of the SCC and SRVM, as demonstrated in the previous works [12], [13], [38].

Furthermore, the total switch count can be reduced by the integration. There are ten switches in total in the conventional system shown in Fig. 3(a) — the PWM buck converter, PV equalizer, and cell equalizer shown in Figs. 4(a)–(c) require two, six, and two switches, respectively —, while the switch count in the proposed integrated converter system is six. In general, each switch requires several ancillary components, including a gate driver IC and its auxiliary power supply, and therefore, a switch count is a good metric to represent circuit complexity. Hence, the circuit-level simplification is feasible due to the reduced total switch count. In addition, according to the previous work [41], in which the total switch stress of the integrated converter is quantitatively compared to that of the conventional system using a PWM converter and SCC-based PV equalizer separately — though a cell equalizer is not included in the comparison —, the analysis revealed that the integrated converter achieves lower total switch stress except for when the duty cycle is extremely low or high. However, it should be cited as a concern that one failure in the integrated converter would cause a malfunction of the system as a whole — e.g. if one of the switches fails, the integrated converter will stop not only PV equalization but also cell equalization from working.

The proposed integrated converter potentially achieves miniaturized design. In contrast to the conventional system that requires two magnetic components (an inductor and transformer for PWM buck converter and SRVM shown in Figs. 4(a) and (c), respectively), the total magnetic component count in the integrated converter as a whole is only one — magnetic components are usually the bulkiest element in switching converters. Furthermore, since the proposed integrated converter is a kind of hybrid SCCs, in which magnetic components can be downsized [42], [43], the magnetic component (i.e., the transformer) in the integrated converter would be smaller than the inductor in a traditional PWM buck converter.

III. Operating Analysis

In this section, the overall operation of the integrated converter is explained first, followed by detailed individual analysis for three key elements listed in Fig 4. Lastly, a dc equivalent circuit of the integrated converter as a whole will be derived to provide an intuitive understanding of how voltages of PV modules and energy storage cells are automatically equalized and to facilitate charge-discharge cycling simulation.

A. Overall Operation

The magnetizing inductance L_{mg} is assumed large enough compared to the leakage inductance L_{kg}. The odd- and even-numbered switches in the SCC are alternately driven, and all the module voltages are automatically unified, similar to the conventional SCC-based equalizers [12], [13]. In the first three modes, the odd- and even-numbered switches are off and on, respectively, and vice versa in the last three modes. The theoretical key operation waveforms and current flow directions when the voltage of B_4, V_4, is the lowest among B_1–B_4 are shown in Figs. 6 and 7, respectively.

In the first mode, Mode 1 [Fig. 7(a)], the applied voltage across the primary winding v_L is $V_{String} - V_{Load}$. The current of L_{mg}, i_{Lmg}, linearly increases provided $L_{mg} >> L_{kg}$. L_{kg} resonates with C_r on the secondary side, producing sinusoidal current (i_{Cr}) flowing through C_4 and D_8 in the SRVM. Therefore, i_{Lkg} is the sinusoidal current superimposed on the triangular current of i_{Lmg}. In the meantime, C_a and C_b in the SCC are connected in parallel with C_{in2} and C_{in3}, respectively, and these capacitors are charged and discharged each other so that voltages of paralleled capacitors become uniform. These parallel connections last by the end of Mode 3.

As i_{Cr} crosses zero, the operation moves to Mode 2 [Fig. 7(b)]. i_{Lmg} is still linearly increasing, while current flow directions on the transformer secondary side are reversed, and D_7 conducts.

When i_{Cr} reaches zero, Mode 3 begins [Fig. 7(c)]. No current flows on the secondary side, while i_{Lmg} is equal to i_{Lkg} and is still linearly increasing. In other words, this operation mode is identical to an on-period of a traditional PWM buck converter.

As the odd- and even-numbered switches are turned-on and -off, respectively, Mode 4 begins [Fig. 7(d)]. The polarity of the voltage applied to the primary winding v_L is reversed as (V_{PV1} + V_{PV2}) − V_{Load}, and i_{Lmg} starts linearly decreasing. Meanwhile, L_{kg} starts resonating with C_r again, inducing sinusoidal current flowing through C_4 and D_7 on the secondary side. In the SCC, C_a and C_b are connected in parallel with C_{in1} and C_{in2}, respectively, starting charging and discharging each other between the paralleled capacitors.

Mode 5 begins as i_{Cr} crosses zero [Fig. 7(e)]. Directions of sinusoidal currents on the secondary side are reversed, and D_8 conducts.

In the final mode, Mode 6 [Fig. 7(f)], the secondary side of the transformer is totally inactive, and hence, this operation mode is essentially identical to an off-period of a traditional PWM buck converter.

Overall, i_{Lmg} is basically a triangular wave similar to a traditional PWM buck converter, while discontinuous sinusoidal current i_{Cr} flows on the secondary side of the SRVM. Hence, i_{Lkg} is equal to i_{Lmg} plus the reflected current of i_{Cr}. Meanwhile, v_L changes between $V_{String} - V_{Load}$ and (V_{PV1} + V_{PV2}) − V_{Load}, and its swing is equal to V_{PV3} (see Fig. 6). The voltage step-down ratio is determined based on the volt-second balance on v_L, as will be explained in Section III-C.

In the SRVM, D_7 and D_8, which are connected in parallel with the least charged cell B_4, conduct while other diodes are off for

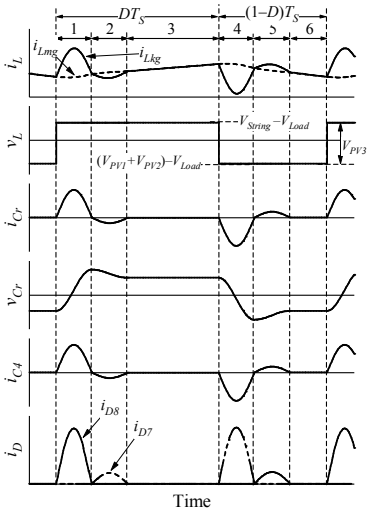

Fig. 6. Theoretical key operation waveforms when V_4 is the lowest in the energy storage source.

the entire period. The average current of C_4 is zero under steady-state conditions, and therefore, the average current of D_7 or D_8 is equal to the equalization current supplied to B_4, I_{eq4} (designated in Fig. 5). Meanwhile, other equalization currents I_{eq1}–I_{eq3} are zero because of no current flowing through other diodes. Although i_{C4} flows through C_{out3} (see Fig. 7), B_3 does not receive I_{eq3} unless D_5 and D_6 conduct. The voltage equalization mechanism of the SRVM will be explained using equivalent circuits in Section III-D.

As mentioned in Section I, the converter for sun-regulated bus systems is active only when PV modules supply power. In other words, B_1–B_4 are equalized only when the integrated converter is active to process the power generated by PV modules. During eclipse periods or at night, on the other hand, B_1–B_4 cannot be equalized because the integrated converter is inactive so B_1–B_4 directly discharge to the load.

As will be discussed in the following subsection, the duty cycle of the upper switches (or even-numbered switches) D varies according to the load voltage V_{Load} and PV module voltage V_{PV}, and therefore, influences of duty cycle variation on the SCC and SRVM should be taken into consideration. In general, SCCs are insensitive to D but slightly influenced; the influence of duty cycle variation on the equalization performance of the SCC will be discussed in Section III-C. Meanwhile, the SRVM can be totally independent of duty cycle variation if the series-resonant tanks is designed so that Modes 3 and 6 exist. The SRVM is essentially inactive, and no current flows on the secondary side during these modes, as can be seen in Figs. 6 and 7. In other words, duty cycle variation is buffered in Modes 3 and 6. To this end, the operation criterion is yielded as

$$1-\frac{f_S}{f_r} > D > \frac{f_S}{f_r}, \tag{1}$$

where f_S is the switching frequency, and f_r is the resonant frequency given by

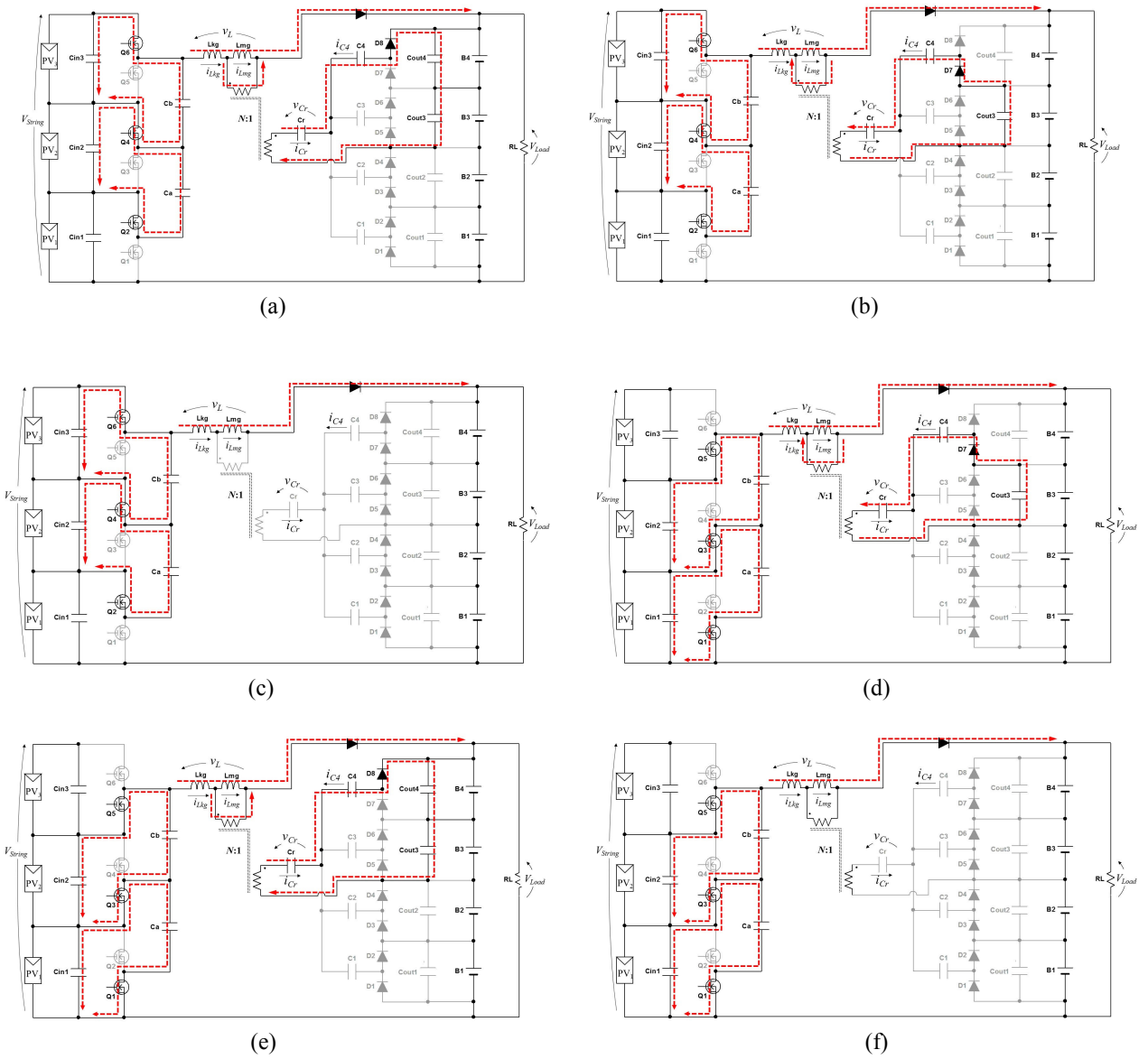

Fig. 7. Current flow directions in (a) Mode 1, (b) Mode 2, (c) Mode 3, (d) Mode 4, (e) Mode 5, and (f) Mode 6.

$$f_r = \frac{1}{2\pi\sqrt{L_{kg}\left(C_r/N^2\right)}}, \tag{2}$$

where N is the transformer turns ratio.

B. PWM Buck Converter

As briefly mentioned in Section III-A, any of switching nodes X–Z in the SCC can be utilized to drive the transformer primary winding, and all PV module voltages are automatically equalized by the SCC even under partial shading conditions. Hence, the voltage at the node of X (Q_5–Q_6) swings between $3V_{PV}$ and $2V_{PV}$. From the volt-second balance on L_{mg}, the voltage step-down ratio of the integrated converter can be yielded as

$$\frac{V_{Load}}{3V_{PV}} = \frac{2+D}{3} \text{ (Node } X\text{)}. \tag{3}$$

In this equation, $3V_{PV}$ that is equal to the string voltage V_{String} (as designated in Fig. 5) corresponds to the input voltage of the PWM buck converter. Similarly, the step-down ratios when nodes Y (Q_3–Q_4) and Z (Q_1–Q_2) are selected can be expressed as

$$\frac{V_{Load}}{3V_{PV}} = \frac{1+D}{3} \text{ (Node } Y\text{)}, \tag{4}$$

$$\frac{V_{Load}}{3V_{PV}} = \frac{D}{3} \text{ (Node } Z\text{)}. \tag{5}$$

Voltage step-down ratios of the integrated converter as a function of duty cycle are compared with that of a traditional PWM buck converter, as shown in Fig. 8. The step-down ratio ranges are dependent on a selected switching node. At a given switching node, the variable step-down ratio range is one-third of that of the traditional buck converter because the total input voltage (i.e. the sum of PV_1–PV_3) is divided into three by the SCC. One of the switching nodes X–Z needs to be properly

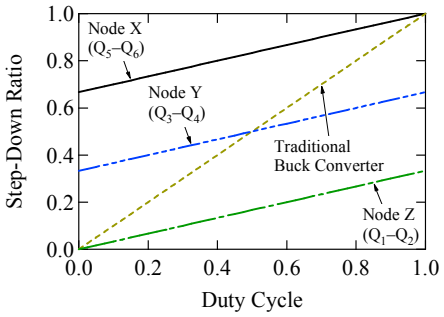

Fig. 8. Voltage step-down ratios as a function of duty cycle.

selected to meet the requirement of voltage conversion ratio in a target application. Otherwise, each module voltage V_{PV} and/or a number of modules connected in series should be adjusted — PV modules for space applications are not commonly standardized, hence allowing V_{PV} to be a design freedom.

During transient periods, such as the start-up when PV modules are not well equalized, V_{PV} and V_{Load} may be out of the step-down range given by (3). However, because the proposed converter is for the sun-regulated system where the energy storage source is directly connected to the load, the load is uninterruptible and is always supported by the energy storage source even during transient periods. Hence, transient behavior of the integrated converter is not of great concern.

C. Switched Capacitor Converter (SCC)

A basic SCC is shown in Fig. 9(a). According to the thorough analysis performed in the previous work [44], the SCC can be equivalently expressed using an ideal transformer with an equivalent resistor R_{eq_a}, as shown in Fig. 9(b). The equivalent resistance value, R_{eq_a}, is given by

$$R_{eq\_a} = \frac{1}{C_a f_S} \frac{\exp\left(\frac{T}{\tau}\right)-1}{\left\{\exp\left(\frac{DT}{\tau}\right)-1\right\}\left\{\exp\left(\frac{(1-D)T}{\tau}\right)-1\right\}}, \qquad (6)$$

where C_a is the capacitance, T (= $1/f_S$) is the switching period, and τ (= $C_a \times r$, where r is the total resistance of the current flow path containing C_a) is the time constant. The value of R_{eq_a} as a function of D is shown in Fig. 9(c); parameters used for the prototype (see Table I) were applied. R_{eq_a} becomes the lowest at D = 0.5 and increases as D moves away from 0.5.

The voltage equalization mechanism of SCCs is well known and analyzed not only for PV modules [12], [13] but also for energy storage cells [24]–[28]. Most conventional SCCs, including resonant and phase-shift versions, are usually operated with a fixed D of 0.5, and this duty cycle condition is optimal from the viewpoint of equalization performance because R_{eq_a} is the lowest at D = 0.5. In the SCC of the proposed integrated converter, on the other hand, R_{eq_a} varies with variable D according to the relationship between V_{PV} and V_{Load}, as expressed by (3). Although the value of R_{eq_a} increases as D moves away from 0.5, it is sufficiently small in a practical duty cycle variation range of, say, 0.1–0.9, suggesting that duty cycle variation does not significantly impair the equalization

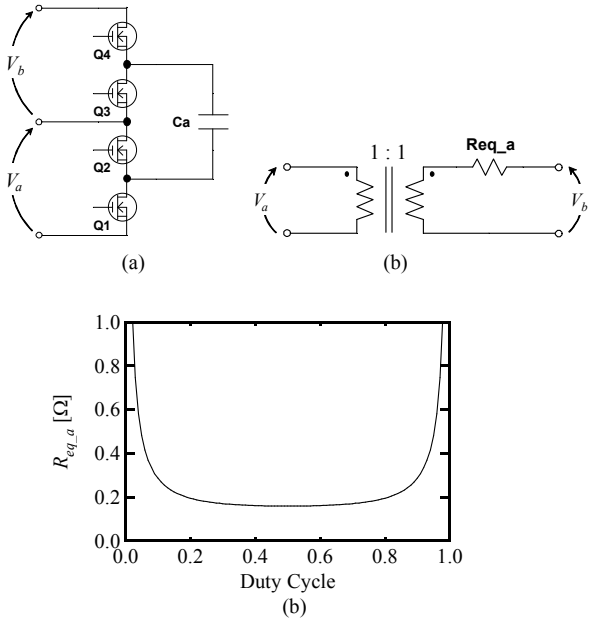

Fig. 9. (a) Basic SCC, (b) equivalent circuit, (c) equivalent resistance as a function of duty cycle.

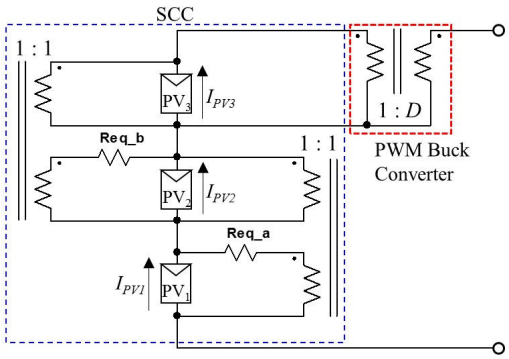

Fig. 10. DC equivalent circuit of SCC equalizer with PWM buck converter.

performance of the SCC in the proposed integrated converter.

From the basic SCC's equivalent circuit shown in Fig. 9(b), a dc equivalent circuit of the SCC equalizer with the PWM buck converter can be obtained, as shown in Fig. 10, in which the PWM converter is depicted as an ideal transformer with the turns ratio of 1:D. Ideal transformers are introduced for PV modules to be connected in series, and all modules are virtually connected in parallel via R_{eq_a} or R_{eq_b} whose resistance value is expressed by (6).

The derived dc equivalent circuit suggests that there would be slight voltage mismatch due to not only voltage drops across R_{eq_a} and R_{eq_b} but also the PWM buck converter partially connected to PV_3. Maximum voltage mismatches at various partial shading conditions as a function of D were investigated using the derived dc equivalent circuit, and results are shown in Fig. 11. PV_1–PV_3 were modeled as constant current sources, and their current values in ampere, which are indicated in parentheses in Fig. 11, represent partial shading conditions. The condition of (1, 2, 3), for example, means that PV_3 is unshaded

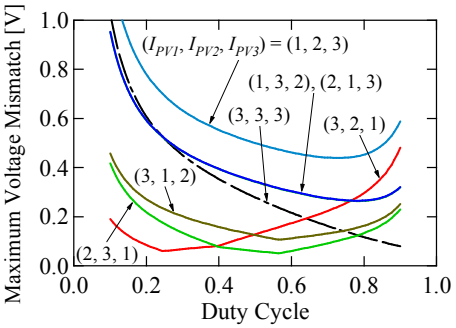

Fig. 11. Maximum PV modules' voltage difference at various partial shading conditions as a function of duty cycle.

while PV_1 and PV_2 are severely and moderately shaded, respectively. It is notable that the unshaded condition of (3, 3, 3) is not the best from the viewpoint of voltage mismatch because of the PWM buck converter partially connected to PV_3. Without the SCC-based equalizer, PV_3 would generate less current than PV_1 and PV_2, and therefore, PV_3-shaded conditions [e.g., (3, 1, 2) and (2, 3, 1)] showed smaller voltage mismatch than the unshaded condition of (3, 3, 3). Voltage mismatches tend to soar as D nears extreme values. In the duty cycle range of 0.2–0.8, the maximum voltage mismatches were lower than 0.8 V.

D. Voltage Equalization Mechanism and Inherent Constant Current Characteristic of SRVM Operating in Discontinuous Conduction Mode (DCM)

The operation of the SRVM in the proposed integrated converter can be analyzed similarly to that in the previous work [38] by assuming $L_{mg} >> L_{kg}$ so that L_{mg} has little influence on the SRVM's operation.

As shown in the inset of Fig. 4(c), the voltage multiplier is driven by a sinusoidal current produced by the series-resonant tank, although the actual waveform is discontinuous sinusoidal current as shown in Fig. 6 (see i_{Cr}). Since all capacitors of C_1–C_4 are connected to the series-resonant tank generating a sinusoidal current, these capacitors are equivalent to coupling capacitors, through which ac components only can flow. From the viewpoint of ac-coupling, B_1–B_4 as well as their corresponding circuit elements can be separated and grounded by removing dc voltage components of C_1–C_4, deriving an ac equivalent circuit shown in Fig. 12. The series-resonant tank is illustrated as an ac current source, and B_2 and B_3 and their corresponding elements are not depicted for the sake of simplicity. From the ac-coupling viewpoint, all dc voltage components, including B_1–B_4 as well as C_{out1}–C_{out4}, may be short-circuited and removed, but they are intentionally unremoved in order to provide an intuitive understanding of the automatic voltage equalization mechanism. In this ac equivalent circuit, B_1–B_4 are virtually connected in parallel through respective capacitor-diode rectifiers (e.g., C_1-D_1-D_2 for B_1), and therefore, the ac current generated by the series-resonant tank is rectified and preferentially supplied to the cell having the lowest voltage among B_1–B_4. In other words, the least charged cell receives an equalization current from the

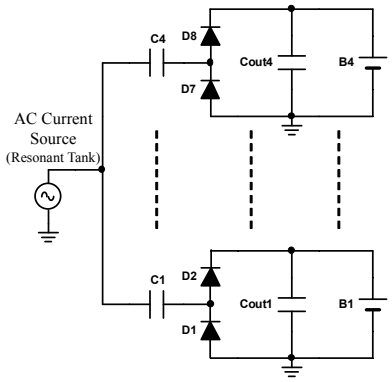

Fig. 12. AC equivalent circuit of SRVM.

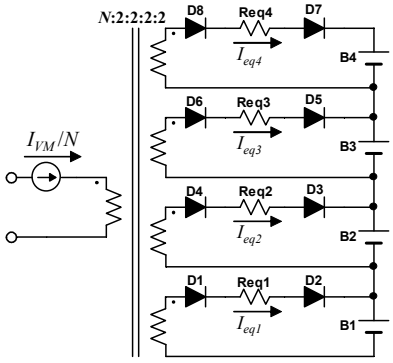

Fig. 13. DC equivalent circuit of SRVM.

SRVM, virtually increasing a charging current for the least charged cell.

The dc equivalent circuit derived based on the detailed analysis in the previous work [38], as shown in Fig. 13, provides more intuitive understanding of how cell voltages are automatically equalized by the SRVM. The SRVM is equivalently expressed using an ideal transformer, diodes, and equivalent resistors whose resistance R_{eqi} is given by

$$R_{eqi} = \frac{1}{2C_i f_S} + \frac{2f_r}{f_S} r_i , \tag{7}$$

where C_i and r_i ($i = 1 \ldots 4$) are the capacitance and ESR of C_1–C_4, respectively. The input current of the SRVM's dc equivalent circuit I_{VM}/N (see Fig. 13) is preferentially distributed to the least charged cell through two diodes and one corresponding equivalent resistor, virtually increasing the charging rate for the least charged cell.

Since energy storage cells are essentially a voltage source, currents supplied from the SRVM to cells should be controlled or limited under a desired level. The previous study has revealed that the SRVM operating in DCM exhibits an inherent constant-current characteristic even without feedback control, and its value is dependent on the voltage swing of the square wave voltage applied to the SRVM's input [38]. In the case of the proposed integrated converter, the voltage swing of the SRVM's input (i.e., peak-to-peak voltage of v_L) is equal to V_{PV3} (= V_{PV}) as designated in Fig. 6. The input current for the dc

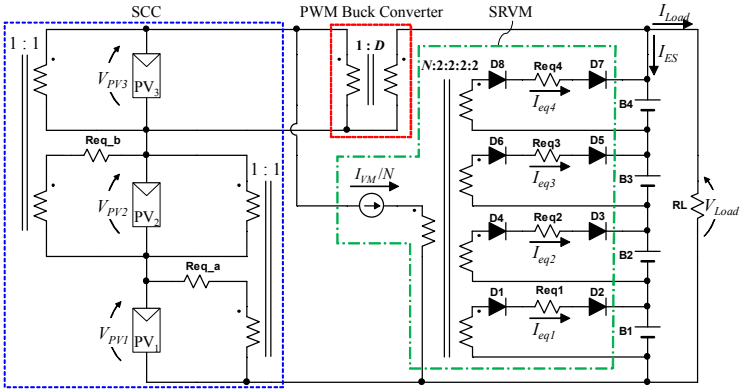

Fig. 14. DC equivalent circuit of proposed integrated converter.

equivalent circuit of the SRVM, I_{VM} is given by

$$I_{VM} \approx \frac{2N\omega_S V_{PV}}{\pi Z_0 \omega_r}, \tag{8}$$

where ω_S and ω_r are the switching and resonant angular frequencies, and Z_0 is the characteristic impedance of the series-resonant tank. This equation suggests that the input current of the SRVM is independent on cell voltages. By designing the series-resonant tank properly so that the SRVM operates in DCM, currents in the SRVM can be limited under desired levels even without feedback control loop, achieving the simplified circuitry by eliminating feedback control loop for the cell equalization from the integrated converter.

E. Derivation of DC Equivalent Circuit

In general, charging and discharging processes take several minutes to hours or even days in practical use. On the other hand, switching frequencies of converters (i.e., chargers, dischargers, and equalizers) are higher than several ten kilohertz. This huge difference in frequency (or period) makes simulation-based charge-discharge cycling using switching converters very time-consuming and impractical — performing 100 kHz-converter simulation for 1-hour charge-discharge cycling would take several hours or even a day. Hence, a dc equivalent circuit containing no high-frequency components is inevitable for charge-discharge cycling simulation.

From the combination of the dc equivalent circuits of the SCC and SRVM shown in Figs. 10 and 13, respectively, a dc equivalent circuit of the proposed integrated converter as a whole can be derived as shown in Fig. 14. The output of the PWM buck converter is tied to the series-connection of the energy storage cells. The SRVM draws current of I_{VM}/N from the input of the PWM buck converter. The values of R_{eq_a} (= R_{eq_b}), R_{eqi}, and I_{VM} can be determined from (6), (7), and (8), respectively, while D of the ideal transformer in the PWM buck converter is adjusted so that the charging current for the series-connected cells, I_{ES}, is controlled. Since no high-frequency switching component exists in this circuit, charge-discharge cycling simulation can be instantly completed.

IV. Experimental Results

A. Prototype

In general, system power requirement for small exploration rovers is less than a few hundred watts. A 100-W prototype of the integrated converter for three PV modules and four energy storage modules was designed and built for typical 28-V bus power systems, as shown in Fig. 15. The SCC equalizer and SRVM including the transformer were separately built for a brief initial check-up and subsequently connected using wires for the integration and experiments. Component values are listed in Table I. The operation condition of the prototype and specifications of PV and energy storage modules for

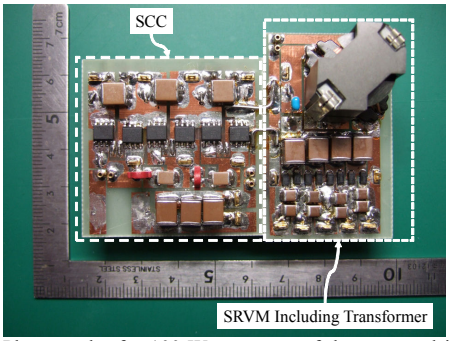

Fig. 15. Photograph of a 100-W prototype of the proposed integrated converter.

TABLE I
COMPONENT VALUES USED FOR THE PROTOTYPE

	Component	Value
SCC	C_1, C_2	Ceramic Capacitor, 33 µF, 5 mΩ
	C_{in1}–C_{in3}	Ceramic Capacitor, 94 µF
	Q_1–Q_8	IRF7477, R_{on} = 6.5 mΩ
	Gate Driver	ISL 6596 (Synchronous Recrified Driver)
SRVM Including Transformer	Transformer	N_1:N_2 = 5:5, L_{kg} = 1.9 µH, L_{mg} = 20.7 µH
	C_r	Ceramic Capacitor, 47 nF
	C_1–C_6	Ceramic Capacitor, 33 µF, 5 mΩ
	C_{out1}–C_{out6}	Ceramic Capacitor, 200 µF
	D_1–D_{12}	Schottky Diode, DFLS220L, V_D = 0.375 V

TABLE II
OPERATION CONDITION OF PROTOTYPE AND SPECIFICATIONS OF PV AND ENERGY STORAGE MODULES

Switching Frequency, f_S	200 kHz
Resonant Frequency, f_r	533 kHz
PV Module	Solar Array Simulator [see Fig. 17(a) for characteristics]
Energy Storage Module	Supercapacitor Module, 220 F
Charging Scheme	CC–CV of 2.0 A–32.0 V (8.0 V/cell)

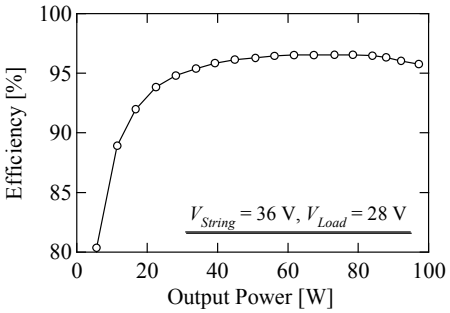

Fig. 16. Measured power conversion efficiency of the prototype under no-partial-shading and no-voltage-imbalance condition.

experiments are shown in Table II.

The power conversion efficiency of the integrated converter as a whole was measured at V_{String} = 36 V and V_{Load} = 28 V under the no-partial-shading and no-voltage-imbalance condition. The result is shown in Fig. 16. The measured efficiency at 100 W output was as high as 95.8%.

B. Equalization for PV Modules

Before testing the integrated performance of the proposed integrated converter as a whole, the equalization performance of the SCC with the PWM buck converter was measured. Solar array simulators (Agilent Technology, E4360A) were used to emulate a partial shading condition; PV_3 is unshaded while PV_1 and PV_2 are moderately and severely shaded, respectively, as depicted in Fig. 17(a). An electronic load operating in constant-voltage mode at 28 V was used instead of energy storage modules B_1–B_4. Duty cycle D was manually varied in the range of 0.15–0.85, which corresponds to V_{String} of approximately 30–40 V according to (3), in order to sweep the string characteristic. As a reference, the string characteristic without equalization was also measured using a variable resistor directly connected to the string.

Measured string characteristics with/without the equalization are shown and compared in Fig. 17(b). Three MPPs, including one global and two local MPPs, were observed in the P–V characteristic without equalization, and the extractable maximum power was merely 42.0 W at V_{String} = 24 V. With equalization, on the other hand, the local MPPs successfully disappeared, and the extractable maximum power considerably increased to as high as 62.8 W at V_{String} = 33 V, demonstrating the equalization performance of the SCC for series-connected PV modules under partial shading.

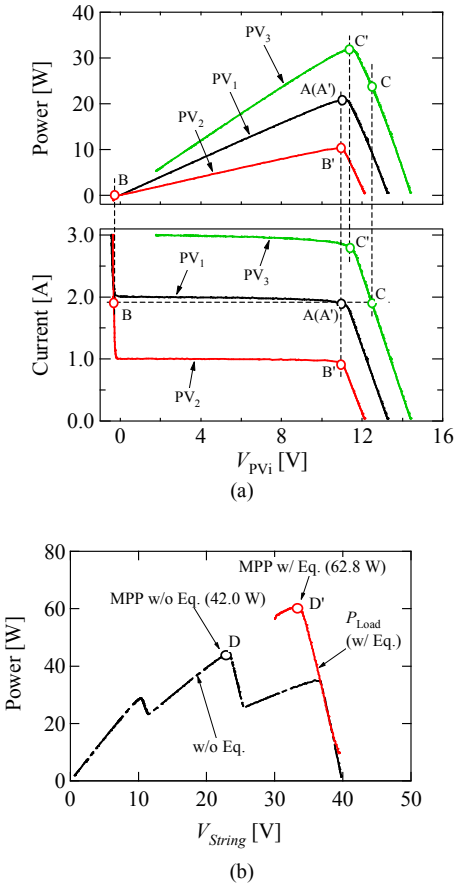

Fig. 17. (a) Individual module characteristics used for experiments, (b) measured string characteristics with/without equalization.

Points A–C and A'–C' in Fig. 17(a) indicate the operation points of individual modules PV_1–PV_3 when the string was operated at D and D' in Fig. 17(b), respectively; A–D and A'–D' are the operation points with and without equalization, respectively. Without equalization, PV_1 was bypassed, and its voltage was the sub-zero value (at B), and the modules' operation voltages at A–C were severely mismatched. With equalization, on the other hand, the operation voltages were nearly unified with small voltage mismatch, allowing all the modules to operate at each near MPP (at A'–C'). The voltages of shaded modules of PV_1 and PV_2 (i.e., A' and B') were slightly lower than that of the unshaded module of PV_3 (C'), and this voltage difference corresponds to the voltage drop across R_{eq_a} and R_{eq_b} in the dc equivalent circuit shown in Figs. 10 and 14.

C. Charge-Discharge Cycling for Series-Connected SC Modules

The SCC equalizer and SRVM including the transformer were combined, as shown in Fig. 15, and the integrated converter was powered by the solar array simulators emulating the partial shading condition shown in Fig. 17(a). A charge-discharge cycling test was performed for the series-connected SC modules, each with a capacitance of 220 F, from an initially-voltage-imbalanced condition. The

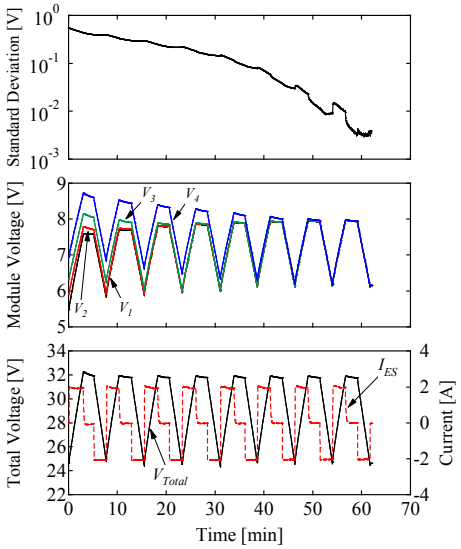

Fig. 18. Resultant cycling profiles of series-connected SC modules.

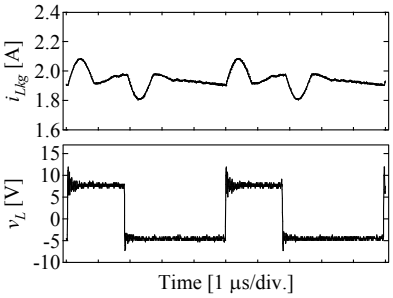

Fig. 19. Measured key operation waveforms during charging in the 1st cycle.

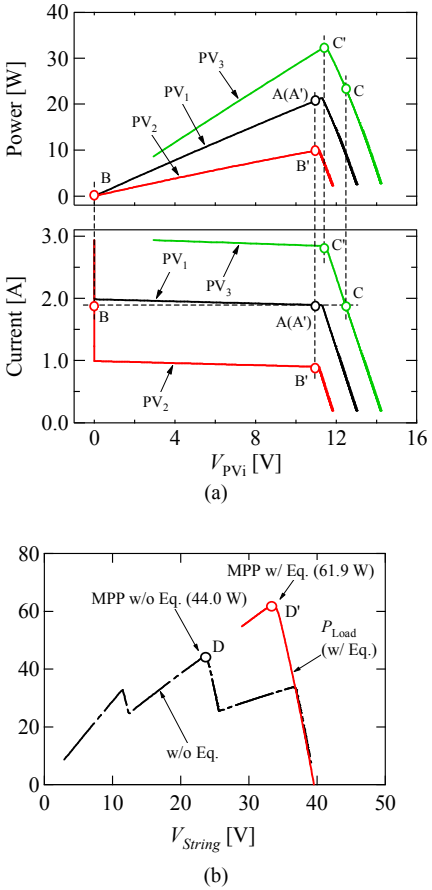

Fig. 20. (a) Individual module characteristics used for equivalent circuit-based simulation, (b) string characteristics with/without equalization.

series-connected SC modules were charged with a constant-current–constant-voltage (CC–CV) charging scheme of 2.0 A–32.0 V (8.0 V/module) using the integrated converter, and was discharged at 2.0 A using an electronic load operating in CC mode.

Resultant cycling profiles are shown in Fig. 18 where V_{Total} (= V_{Load}) is the total voltage of the series-connected SC modules and I_{ES} is the current of the energy storage string (see Fig. 5). In the first few cycles, modules of B_3 and B_4 (V_3 and V_4 in the middle panel of Fig. 18) were over-charged because of their high initial voltages. As the cycling progressed, the voltage imbalance was gradually eliminated, and the standard deviation of module voltages steadily decreased thanks to the SRVM's preferential equalization current distribution to the least charged module, as explained in Section III-D. In the last few cycles, fluctuation in the standard deviation was observed, and it is attributable to the minor mismatch in capacitance of the series-connected SC modules — capacitance mismatch naturally causes voltage imbalance during cycling. In the 8th cycle, all module voltages were adequately unified, and the standard deviation at the end of the cycling was as low as 3 mV, demonstrating the voltage equalization performance of the integrated converter.

Measured key waveforms during charging in the 1st cycle are shown in Fig. 19. The voltage across the primary winding, v_L, was square wave voltage, while the measured i_{Lkg} was a triangular wave with the superimposed discontinuous sinusoidal wave, similar to the theoretical waveforms shown in Fig. 6.

V. Simulation Analysis

The simulation analysis based on the derived dc equivalent circuit shown in Fig. 14 was also performed emulating the same partial-shading, initial voltage imbalance, and charge-discharge cycling conditions as the experiments. The values of R_{eq_a} (= R_{eq_b}) and R_{eqi} were determined to be 200 mΩ and 182 mΩ, respectively, according to (6) [or Fig. 9(c)] and (7). A single-diode equivalent model [45] was employed to emulate the individual PV module characteristics.

The simulation results of the PV module equalization are shown in Fig. 20. The simulation results matched very well with the experimental results shown in Fig. 17, verifying the derived dc equivalent circuit.

The simulation results of the charge-discharge cycling test is shown in Fig. 21. Resultant cycling profiles of module voltages agreed well with the experimental ones shown in Fig. 18. The standard deviation profile of the simulation was clearer than that of the experiment because of no capacitance mismatch that

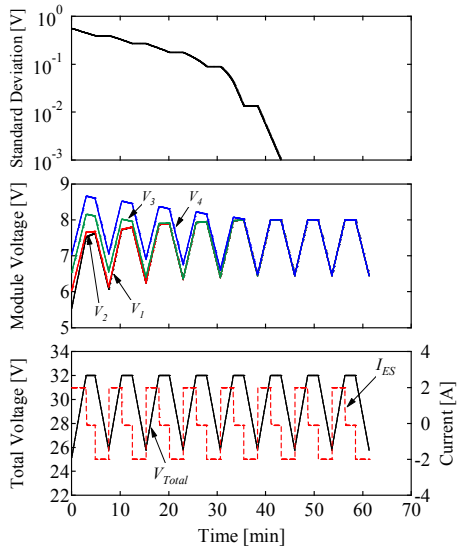

Fig. 21. Simulation cycling profiles of series-connected SC modules.

causes minor voltage imbalance originating from cycling. The standard deviation steadily declined during charging thanks to the voltage equalization by the SRVM. During discharging, on the other hand, it kept constant as the series-connected SCs were directly discharged with a CC load. The standard deviation in the experiment decreased down to approximately 3 mV at the end of the cycling test (see Fig. 18), while it consistently fell even below 1 mV in the simulation because of no capacitance mismatch.

VI. Conclusions

The PWM converter integrating voltage equalizers for series-connected PV modules and energy storage cells has been proposed for exploration rovers in this paper. The proposed integrated converter is basically the combination of the PWM buck converter, SCC-based PV equalizer, and SRVM-based cell equalizer. Three functional components are integrated into a single unit with reducing the total switch count, achieving not only system-level but also circuit-level simplifications. In addition, the magnetic component count necessary in the proposed integrated converter is only one, potentially achieving the miniaturized design. The derivation procedure of the proposed integrated converter was explained, followed by the operation analysis and derivation of the dc equivalent circuit that contributes to reduced simulation burden and time.

The experimental charge-discharge cycling test was performed emulating a partially-shaded condition for series-connected SC modules from the initially voltage-imbalanced condition. With the proposed integrated converter, not only was the extractable maximum power from PV modules significantly increased but also voltage imbalance of SC modules was adequately eliminated after several charge-discharge cycles, demonstrating the integrated performance of the proposed integrated converter. The simulation-based charge-discharge cycling using the derived dc equivalent circuit was also performed under the same conditions as the experiments. The experimental and simulation results matched very well, verifying the derived dc equivalent circuit.

References

[1] S. Poshtkouhi, V. Palaniappan, M. Fard, and O. Trescases, "A general approach for quantifying the benefit of distributed power electronics for fine grained MPPT in photovoltaic applications using 3-D modeling," *IEEE Trans. Power Electron*., vol. 27, no. 11, pp. 4656–4666, Nov. 2012.

[2] M. Vitelli, "On the necessity of joint adoption of both distributed maximum power point tracking and central maximum power point tracking in PV systems," Prog. Photovolt. Res. Appl., vol. 22, pp. 283-299, 2014.

[3] P. S. Shenoy, K. A. Kim, B. B. Johnson, and P. T. Krein, "Differential power processing for increased energy production and reliability of photovoltaic systems," *IEEE Trans. Ind. Power Electron*., vol. 28, no. 6, pp. 2968–2979, Jun. 2013.

[4] H. J. Bergveld, D. Büthker, C. Castello, T. Doorn, A. D. Jong, R. V. Otten, and K. D. Waal, "Module-level dc/dc conversion for photovoltaic systems: the delta-conversion concept," *IEEE Trans. Power Electron*., vol. 28, no. 4, pp. 2005–2013, Apr. 2013.

[5] M. S. Zaman, Y. Wen, R. Fernandes, B. Buter, T. Doorn, M. Dijkstra, H. J. Bergveld, and O. Trescases, "A cell-level differential power processing IC for concentrating-PV systems with bidirectional hysteretic current-mode control and closed-loop frequency regulation," *IEEE Trans. Power Electron*., vol. 28, no. 6, pp. 2936–2945, Jun. 2013.

[6] S. Qin, S. T. Cady, A. D. D. García, and R. C. N. P. Podgurski, "A distributed approach to maximum power point tracking for photovoltaic submodule differential power processing," *IEEE Trans. Power Electron*., vol. 30, no. 4, pp. 2024–2040, Apr. 2015.

[7] L. F. L. Villa, T. P. Ho, J. C. Crebier, and B. Raison, "A power electronics equalizer application for partially shaded photovoltaic modules," *IEEE Trans. Ind. Electron*., vol. 60, no. 3, pp. 1179–1190, Mar. 2013.

[8] L. F. L. Villa, X. Pichon, F. S. Ardelibi, B. Raison, J. C. Crebier, and A. Labonne, "Toward the design of control algorithms for a photovoltaic equalizer: choosing the optimum switching strategy and the duty cycle," *IEEE Trans. Power Electron*., vol. 29, no. 3, pp. 1447–1460, Mar. 2014.

[9] M. Z. Ramli and Z. Salam, "A simple energy recovery scheme to harvest the energy from shaded photovoltaic modules during partial shading," *IEEE Tran. Power Electron*., vol. 29, no. 12, pp. 6458–6471, Dec. 2014.

[10] T. Shimizu, O, Hashimoto, and G. Kimura, "A novel high-performance utility-interactive photovoltaic inverter system," *IEEE Trans. Power Electron*., vol. 18, no. 2, pp. 704–711, Mar. 2003.

[11] T. Shimizu, M. Hirakata, T. Kamezawa, and H. Watanabe, "Generation control circuit for photovoltaic modules," *IEEE Trans. Power Electron*., vol. 16, no. 3, pp. 293–300, May 2001.

[12] J. T. Stauth, M. D. Seeman, and K. Kesarwani, "Resonant switched-capacitor converters for sub-module distributed photovoltaic power management," *IEEE Trans. Power Electron*., vol. 28, no. 3, pp. 1189–1198, Mar. 2013.

[13] S. B. Yaakov, A. Blumenfeld, A. Cervera, and M. Evzelman, "Design and evaluation of a modular resonant switched capacitor equalizer for PV panels," in Proc. *IEEE Energy Conversion Cong. Expo*., pp. 4129–4136, 2012.

[14] C. Olalla, D. Clement, M. Rodríguez, and D. Makisimović, "Architectures and control of submodule integrated dc-dc converters for photovoltaic applications," *IEEE Trans. Power Electron*., vol. 28, no. 6, pp. 2980–2997, Jun. 2013.

[15] C. Olalla, C. Deline, D. Clement, Y. Levron, M. Rodríguez, and D. Makisimović, "Performance of power limited differential power processing architectures in mismatched PV systems," *IEEE Trans. Power Electron*., vol. 30, no. 2, pp. 618–631, Feb. 2015.

[16] M. Uno and A. Kukita, "Two-switch voltage equalizer using an LLC resonant inverter and voltage multiplier for partially-shaded series-connected photovoltaic modules," *IEEE Trans. Ind. Appl*., vol. 51, no. 2, Mar/Apr. 2015, pp. 1587–1601.

[17] M. Uno and A. Kukita, "Single-switch voltage equalizer using multi-stacked buck-boost converters for partially-shaded photovoltaic modules," *IEEE Trans. Power Electron*., vol. 30, no. 6, Jun. 2015, pp. 3091–3105.

[18] M. Uno and A. Kukita, "Accelerated charge-discharge cycling test and cycle life prediction model for supercapacitors in alternative battery applications," *IEEE Trans. Ind. Electron*., vol. 59, no. 12, Dec. 2012, pp. 4704–4712.
[19] M. Uno and A. Kukita, "Cycle life evaluation based on accelerated aging testing for lithium-ion capacitors as alternative to rechargeable batteries," IEEE Trans. Ind. Electron., vol. 63, no. 3, Mar. 2016, pp. 1607–1617.
[20] R. Kötz, P.W. Ruch, and D. Cericola, "Aging and failure mode of electrochemical double layer capacitors during accelerated constant load tests," *J. Power Sources*, vol. 195, no. 3, pp. 923–928, Feb. 2010.
[21] P. A. Cassani and S. S. Williamson, "Feasibility analysis of a novel cell equalizer topology for plug-in hybrid electric vehicle energy-storage systems," *IEEE Trans. Veh. Technol*., vol. 58, no. 8, Oct. 2009, pp. 3938–3946.
[22] P. A. Cassani and S. S. Williamson, "Design, testing, and validation of a simplified control scheme for a novel plug-ion hybrid electric vehicle battery cell equalizer," *IEEE Trans. Ind. Electron*., vol. 57, no. 12, Dec. 2010, pp. 3956–3962.
[23] T. H. Phung, A. Collet, and J. Crebier, "An optimized topology for next-to-next balancing of series-connected lithium-ion cells," *IEEE Trans. Power Electron*., vol. 29, no. 9, Sep. 2014, pp. 4603–4613.
[24] A. Baughman and M. Ferdowsi, "Double-tiered switched-capacitor battery charge equalization technique," *IEEE Trans. Ind. Appl*., vol. 55, no. 6, Jun. 2008, pp. 2277–2285.
[25] H. S. Park, C. H. Kim, K. B. Park, G. W. Moon, and J. H. Lee, "Design of a charge equalizer based on battery modularization," *IEEE Trans. Veh. Technol*., vol. 58, no. 7, Sep. 2009, pp. 3216–3223.
[26] M. Uno and K. Tanaka, "Influence of high-frequency charge-discharge cycling induced by cell voltage equalizers on the life performance of lithium-ion cells," *IEEE Trans. Veh. Technol*., vol. 60, no. 4, May 2011, pp. 1505–1515.
[27] Y. Yuanmao, K. W. E. Cheng, and Y. P. B. Yeung, "Zero-current switching switched-capacitor zero-voltage-gap automatic equalization system for series battery string," IEEE Trans. Power Electron., vol. 27, no. 7, Jul. 2012, pp. 3234–3242.
[28] M. Y. Kim, C. H. Kim, J. H. Kim, and G. W. Moon, "A chain structure of switched capacitor for improved cell balancing speed of lithium-ion batteries," *IEEE Trans. Ind. Electron*., vol. 61, no. 9, Aug. 2014, pp. 3989–3999.
[29] S. H. Park, K. B. Park, H .S. Kim, G. W. Moon, and M. J. Youn, "Single-magnetic cell-to-cell charge equalization converter with reduced number of transformer windings," *IEEE Trans. Power Electron*., vol. 27, no. 6, Jun. 2012, pp. 2900–2911.
[30] C. S. Lim, K. J. Lee, N. J. Ku, D. S. Hyun, and R. Y. Kim, "A modularized equalization method based on magnetizing energy for a series-connected lithium-ion battery string," *IEEE Trans. Power Electron*., vol. 29, no. 4, Apr. 2014, pp. 1791–1799.
[31] A. M. Imtiaz, F. H. Khan, and H. Kamath, "Time shared flyback converter" based regenerative cell balancing technique for series connected Li-ion battery strings," *IEEE Trans. Power Electron*., vol. 28, no. 12, Dec. 2013, pp. 5960–5975.
[32] C. H. Kim, M. Y. Kim, and G. W. Moon, "A modularized charge equalizer using a battery monitoring IC for series-connected Li-ion battery strings in electric vehicles," *IEEE Trans. Power Electron*., vol. 28, no. 8, Aug. 2013, pp. 3779–3787.
[33] M. Uno and K. Tanaka, "Single-switch cell voltage equalizer using multistacked buck–boost converters operating in discontinuous conduction mode for series-connected energy storage cells," *IEEE Trans. Veh. Technol*., vol. 60, no. 8, Oct. 2011, pp. 3635–3645.
[34] M. Uno and K. Tanaka, "Double-switch single-transformer cell voltage equalizer using a half-bridge inverter and voltage multiplier for series-connected supercapacitors," *IEEE Trans. Veh. Technol*., vol. 61, no. 9, Nov. 2012, pp. 3920–3930.
[35] M. Uno and A. Kukita, "Double-switch equalizer using parallel- or series-parallel-resonant inverter and voltage multiplier for series-connected supercapacitors," *IEEE Trans. Power Electron*., vol. 29, no. 2, Feb. 2014, pp. 812–828.
[36] M. Uno and K. Tanaka, "Single-switch multi-output charger using voltage multiplier for series-connected lithium-ion battery/supercapacitor equalization," *IEEE Trans. Ind. Electron*., vol. 60, no. 8, Aug. 2013, pp. 3227–3239.
[37] M. Uno and A. Kukita, "PWM switched capacitor converter integrating voltage equalizers for series-connected energy storage cells and photovoltaic modules," in Proc. *IEEE Int. Conf. Power Electron. (ICPE)*, ECCE-Asia, pp. 1889–1896, Jun. 2015.
[38] M. Uno and A. Kukita, "Bidirectional PWM converter integrating cell voltage equalizer using series-resonant voltage multiplier for series-connected energy storage cells," *IEEE Trans. Power Electron*., vol. 30, no. 6, Jun. 2015, pp. 3077–3090.
[39] M. Uno and A. Kukita, "Cell voltage equalizer using series resonant inverter and voltage multiplier for series-connected supercapacitors," in Proc. *IEEE Energy Conversion Cong. Expo*., pp. 672–677, 2012.
[40] TDK. (2010, Sep.) LLC Resonant Power Transformers. [Online]. available: http://www.ic-contract.ru/images/pdf/TDK/e636_srx.pdf#search='TDK +LLC+transformer
[41] M. Uno and A. Kukita, "PWM converter integrating switched capacitor voltage equalizer for photovoltaic modules under partial shading," in Proc. *IEEE EPE'15 ECCE Europe*, pp. 1–10, 2015.
[42] S. R. Sanders, E. Alon, H. P. Le, M. D. Seeman, M. Jhon, and V. W. Ng, "The road to fully integrated DC-DC conversion via the switched-capacitor approach," *IEEE Trans. Power Electron*., vol. 28, no. 9, pp. 4146–4155, Sep. 2013.
[43] M. Uno, "High step-down converter integrating switched capacitor converter and PWM synchronous buck converter," in Proc. *IEEE Int. Telecommun. Energy Conf. (INTELEC)*, pp. 2736–278, Oct. 2013.
[44] J. W. Kimball, P. T. Krein, and K. R. Cahill, "Modeling of capacitor impedance in switching converters," *IEEE Power Electron. Lett*., vol. 3, pp. 136–140, Dec. 2005.
[45] S. M. MacAlpine, R. W. Erickson, and M. J. Brandemuehl, "Characterization of power optimizer potential to increase energy capture in photovoltaic systems operating under nonuiform conditions," *IEEE Trans. Power Electron*., vol. 28, no. 6, pp. 2936–2945, Jun. 2013.

Masatoshi Uno (M'06) was born in Japan in 1979. He received the B.E. degree in electronics engineering and the M.E. degree in electrical engineering from Doshisha University, Kyoto, Japan, and the Ph.D. degree in space and astronautical science from the Graduate University for Advanced Studies, Hayama, Japan, in 2002, 2004, and 2012, respectively. In 2004, he joined the Japan Aerospace Exploration Agency, Sagamihara, Japan, where he developed spacecraft power systems including battery, photovoltaic, and fuel cell systems. In 2014, he joined the Department of Electrical and Electronics Engineering, Ibaraki University, Ibaraki, Japan, where he is currently an Associate Professor of Electrical Engineering. His research interests include switching power converters, cell equalizers, life evaluation for supercapacitors and lithium-ion batteries, and development of fuel cell systems. Dr. Uno is a member of the Institute of Electrical Engineers of Japan (IEEJ) and the Institute of Electronics, Information, and Communication Engineers (IEICE).

M. Uno is a member of the Institute of Electrical Engineering of Japan (IEEJ), and the Institute of Electronics, Information and Communication Engineers (IEICE).

Akio Kukita was born in Japan in 1967. He received the B.E. degree in physics from Chuo University, Japan, in 1993.

From 1993 to 1996 and 1996 to 2008, he was with SEIKO Holdings Corporation and Ebara Corporation, respectively. Since 2008, he has been with Japan Aerospace Exploration Agency as a senior engineer. His recent work has focused on the development of spacecraft power systems.